Electronic Supporting Information

Electrocatalytic Oxidation of Ethanol and Ethylene Glycol on Cubic, Octahedral and Rhombic Dodecahedral Palladium Nanocrystals

Xian-Yin Ma[a,c], Yafeng Chen[b], Han Wang[c], Qiao-Xia Li[a], Wen-Feng Lin[b,*], Wen-Bin Cai[c,a*]

a Shanghai Key Laboratory of Materials Protection and Advanced Materials in Electric Power, College of Environmental and Chemical Engineering, Shanghai University of Electric Power, Shanghai 200090, China
b Department of Chemical Engineering, Loughborough University, Loughborough, Leicestershire, LE11 3TU, U.K.
c Shanghai Key Laboratory of Molecular Catalysis and Innovative Materials, Collaborative Innovation Center of Chemistry for Energy Materials, Department of Chemistry, Fudan University, Shanghai 200433, China

* Corresponding author. Tel.: +44 (0)1509 222 506; E-mail: W.Lin@lboro.ac.uk.
* Corresponding author. Tel.: +86 21 55664050; E-mail: wbcai@fudan.edu.cn.

1. *Material synthesis and electrochemical measurement*

Pd cubes, RDs and Octs were prepared with one-pot synthesis. Briefly, 50 μL of 1 mM KI solution and 500 μL of 10 mM H_2PdCl_4 solution were subsequently added under magnetic stirring at 250 rpm to 10 mL of 25.0 mM cetyltrimethylammonium bromide (CTAB) solution pre-heated to 95 °C in an oil bath. Then, 80 μL of 100 mM ascorbic acid (AA) solution was injected into the above mixed solution and the reaction was allowed to proceed for 30 min until Pd RDs formed. The synthesis of Pd cubes followed the same procedures except that the CTAB concentration was lowered to 12.5 mM without addition of KI.[1, 2] In preparing Pd Octs,[3] 4 mL of 50 mM Na_2PdCl_4 solution was injected under vigorous stirring to 7 mL of a mixed aqueous solution containing 115 mM cetyltrimethylammonium chloride (CTAC), 45 mM citric acid and 50 mM AA pre-heated to 100 °C. The reaction was allowed to proceed for 3 h until Pd Octs formed. The as-synthesized Pd nanocrystals were collected and pre-cleaned through repeated centrifugation (9000 rpm, 10 min) and re-dispersion into ultrapure water for 3 times. Finally, Pd cubes and RDs were concentrated to a colloid of ca. 150 μL and Pd Octs to a colloid of ca. 3 mL. 5.6 μL of a thus-obtained colloid was casted on a glassy carbon electrode (ϕ=3 mm) as the working electrode for further electrochemical surface cleaning and measurement in a typical three-compartment glass cell. A saturated calomel electrode (SCE) and a Pt foil were used as the reference and counter electrodes, respectively. The electrolytes were prepared by dissolving high purity NaOH and H_2SO_4 in Milli-Q ultrapure water, and deaerated with high purity N_2 or CO before an electrochemical measurement.

2. TEM images and edge length distribution histograms of Pd nanocrystals

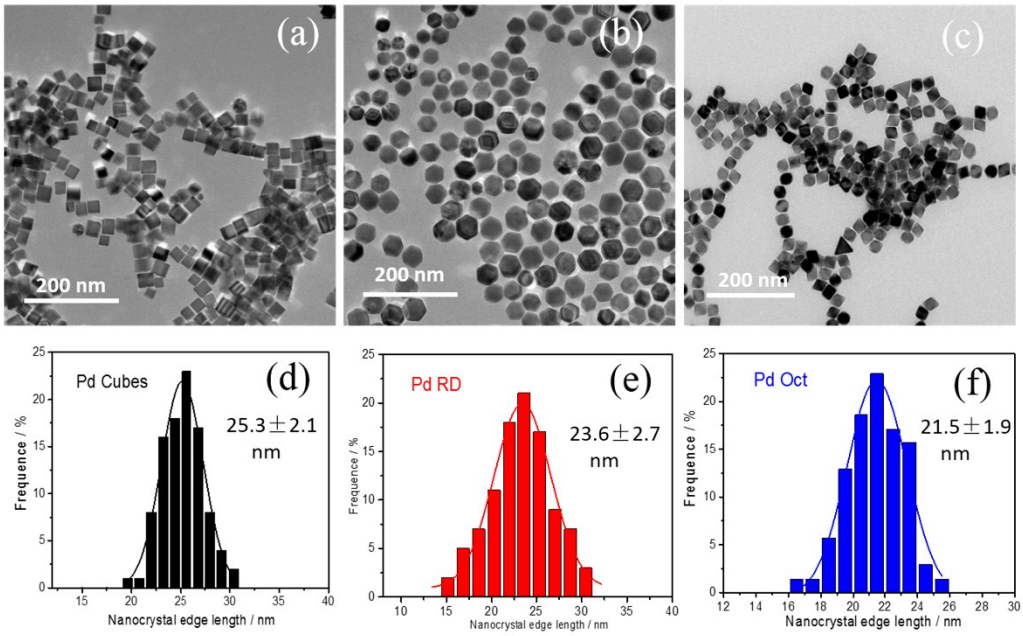

Figure S1. TEM images of Pd cubes (a), RDs (b) and Octs (c) at the scale bar of 200 nm and nanocrystal edge length distribution histograms for Pd cubes (d), RDs (e) and Octs (f). The edge length of as-synthesized Pd Cubes, Pd RDs and Pd Octs is 25.3±2.1 nm, 23.6±2.7 nm and 21.5±1.9 nm, respectively.

3. High-resolution transmission electron microscopic (HRTEM) images and selected area electron diffraction (SAED) images of Pd Cubes, Pd RDs and Pd Octs

The HRTEM images of Pd Cubes (Figs. S2a and d), Pd RDs (Figs. S2 b and e) and Pd Octs (Figures S2c and f) show the d spacing of 1.96 Å, 2.61 Å and 2.22 Å for adjacent lattice fringes corresponding to that of the {100} {110} and {111} planes of an *fcc* Pd crystal, respectively. The selected area electron diffraction (SAED) patterns of Pd Cubes (Figure S2h), Pd RDs (Figure S2i) and Pd Octs (Figure S2j) demonstrates their single crystal nature, respectively.

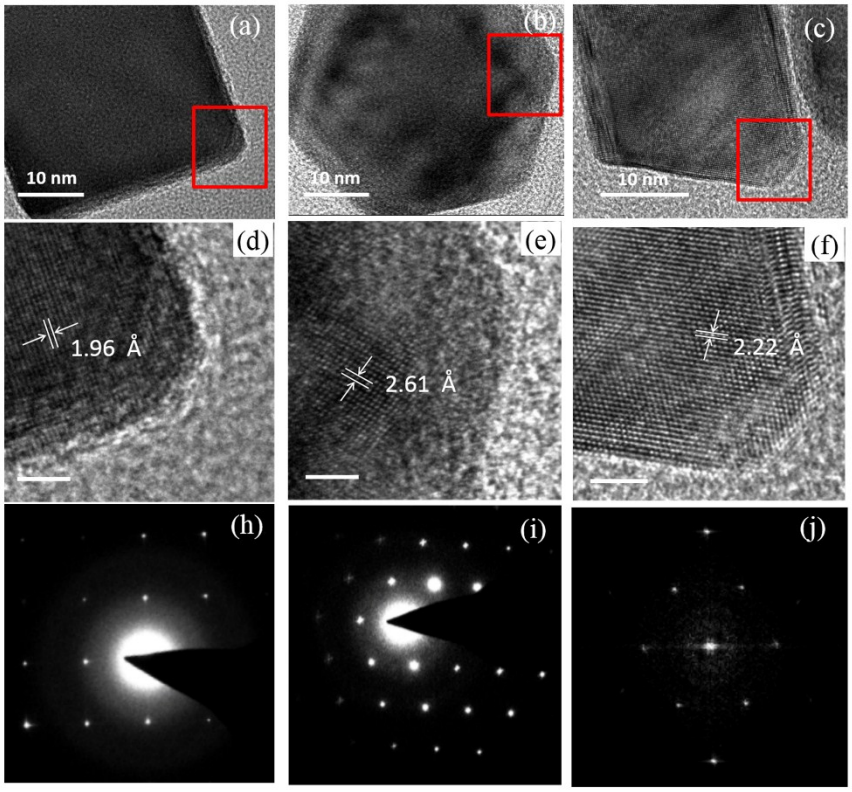

Figure S2. The high-resolution transmission electron microscopic (HRTEM) images of Pd cubes (a), RDs (b) and Octs (c) at the scale bar of 10 nm (d, e and f); The corresponding zoomed images of the regions marked in a, b and c with red rectangles. Selected area electron diffraction (SAED) images of Pd cubes (h), RDs (i) and Octs (j).

4. XRD images of the three types of Pd nanocrystals

Figure S3 shows the XRD spectra recorded for evaluation of the crystal structures of the prepared Pd nanocatalysts. As expected, Pd Cubes and Octs exhibited the strongest characteristic diffraction peaks featuring the (200) and (111) planes, respectively; whilst Pd RDs showed clearly the (220) plane. The fact that the peaks featuring the (111) and (200) planes are also shown from the Pd RDs samples is due to the situation that it was very difficult to obtain an ordered structure for Pd RDs at flat and polished glass substrate by self-assemble in comparison to Pd cube and Pd Octs. The reasons for the latter may be comprehended by the fact that the geometry of Pd RDs with twelve {110} nanofacets is relatively more close to that of round-shaped nanoparticles, and thus Pd RDs are hard to be oriented with one of nanofacets being parallel to the flat substrate as we wished.

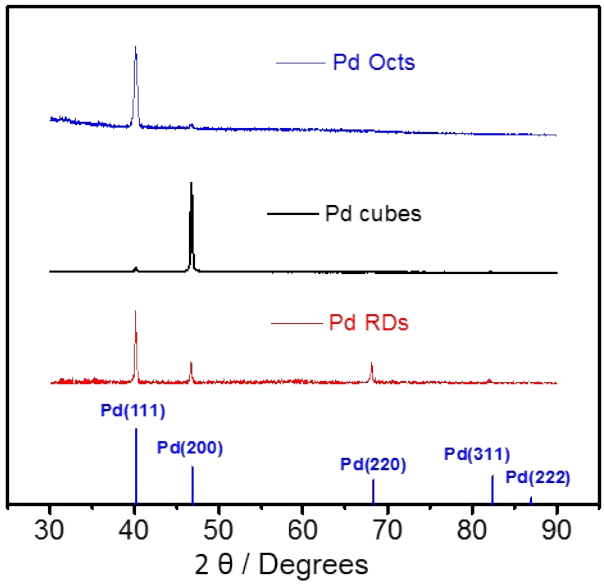

Figure S3. XRD patterns of Pd cubes (black), Octs (blue) and RDs (red).

5. Cyclic voltammograms (CVs) for the three Pd nanocrystals before and after cleaning process

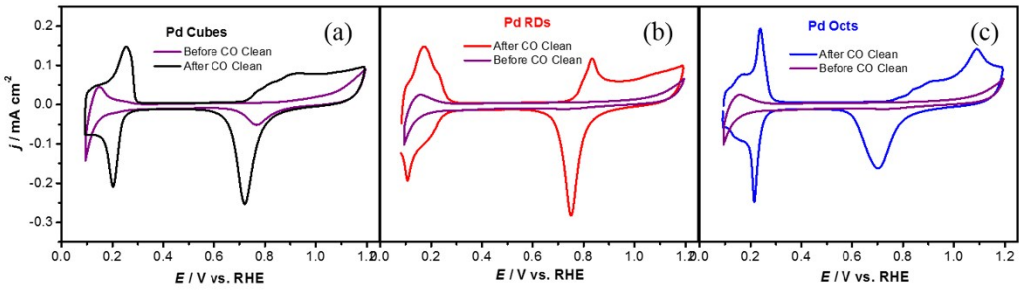

Figure S4. Cyclic voltammograms for Pd Cubes (a), Pd RDs (b) and Pd Octs (c) in 0.5 M H_2SO_4 before and after cleaning the surfaces by CO adsorption−displacement treatment. Scan rate: 50 mV s^{-1}. The current densities indicated are obtained by normalizing respectively the measured currents to the electroactive areas of Pd nanocrystals.

6. Cyclic voltammograms (CVs) of Pd cubes before and after EGOR test

In the electrochemical system, the stability of Pd facet structures largely depends on the applied potential and the holding time, not only for Pd nanocrystals but also for Pd bulk single crystals. To prevent any significant destruction of the crystalline facet structure, the upper limited potential was restricted to only 1.15 V vs. RHE in the CV measurements for EOR and EGOR with a normal scan rate of 50 mV s^{-1}. For the chronoamperometric measurement, the potentials were held at much lower potentials such as 0.65 V and 0.82 V.

The surface structure sensitive cyclic voltammograms (CVs) may provide a useful diagnosis to the surface structural change of Pd nanocrystals. The largely overlapped CVs for Pd nanocubes in 0.5 M H_2SO_4 acquired before and after EGOR test (see Figure S5) reveal that this surface structural change, if any, is minor under the experimental conditions we performed.

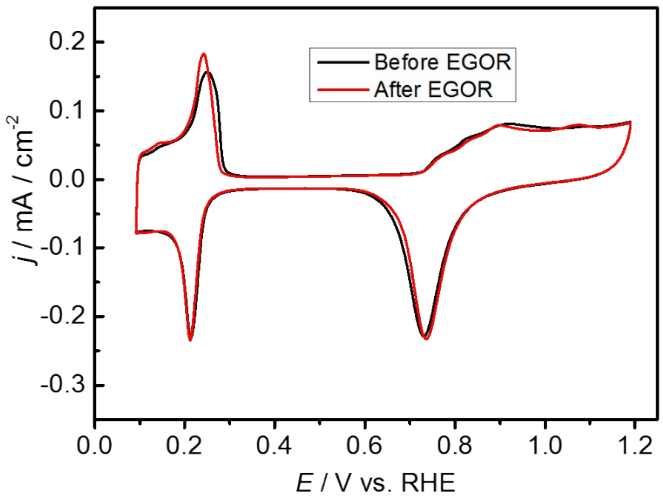

Figure S5. Cyclic voltammograms (CVs) of Pd cubes recorded in 0.5 M H_2SO_4 at 50 mV s^{-1} before (black line) and after (red line) EGOR test.

7. *Density functional theory (DFT) computational method*

All the electronic structure calculations were carried out using the Vienna Ab-initio Simulation Package (VASP) with Perdew–Burke–Ernzerhof (PBE) and generalized gradient approximation (GGA). The project-augmented wave (PAW) pseudopotentials were utilized to describe the core-valence electron interaction.[4-11] The cut-off energy for system convergence was set to 400 eV. Pd(100), Pd(110) and Pd(111) surfaces were all modeled by a p(2 × 2) unit cell with four-layer slabs. The bottom two layers were fixed in geometry, whilst the top two layers and any adsorbates were allowed to relax. A ~ 12 Å vacuum region was applied to ensure interaction between slabs and a 3 × 3 × 1 Monkhorst-Pack k-point sampling was used for Brillouin zone. The calculated equilibrium lattice parameter of Pd is 3.950 Å. The 4 × 4 × 1, 5 × 5 × 1 and 6 × 6 × 1 k-point samplings for Brillouin zone integration had been tested, the differences of the energy results were less than 0.03 eV. The formation of surface oxidant OH^* from water adsorption and oxidation on the three facets was simulated using a simplified model of ¼ monolayer of OH_{ads}, with the optimized and most stable adsorption sites shown in Figure S5, whilst the adsorption energies for all possible sites are list in the Table S1. In this paper, the adsorption energy was defined as: E_{ad} = E(adsorbate/surface) - E(adsorbate) - E(surface), where E(adsorbate/surface), E(adsorbate), and E(surface) are the total energies of the adsorbate binding with the metal surface, gaseous adsorbate and clean surface, respectively. From the adsorption energy data as shown in the Table S1, the most stable adsorption sites of OH_{ads} on the three facets are all bridge sites.

For the calculation of the OH* formation potential derived from water dissociation[12-15], $H_2O \rightarrow OH^* + H^+ + e^-$, the reaction free energy (ΔG) of the OH* formation was calculated by using $\Delta G = \Delta E + \Delta ZPE - T\Delta S$, in which E is the total energy of species, S is the entropy and ZPE is the zero point energy at room temperature. Thus, the reaction free energy for the water splitting reaction was written as: $\Delta G = G(OH^*) + G(H^+ + e^-) - G(H_2O)$. At the electrode potential of 0 V, pH = 0 ($[H^+]$ = 1 M) and the room temperature at 298 K, the free energy of $H^+ + e^-$ can be

replaced by the free energy of ½ H_2, due to the equilibrium of $H^+ + e^- \rightarrow 1/2\ H_2$, under standard hydrogen electrode (SHE) condition. Two correction terms were essential to be added: the electrode potential (eU) referring to a standard hydrogen electrode (SHE) and the pH of an aqueous solution (pH k T ln10), resulting in $G(H^+ + e^-) = G(1/2\ H_2)$ – pH k T ln10 + eU. When $\Delta G = 0$, the water dissociation reaction was in equilibrium and the OH* formation potential was obtained.

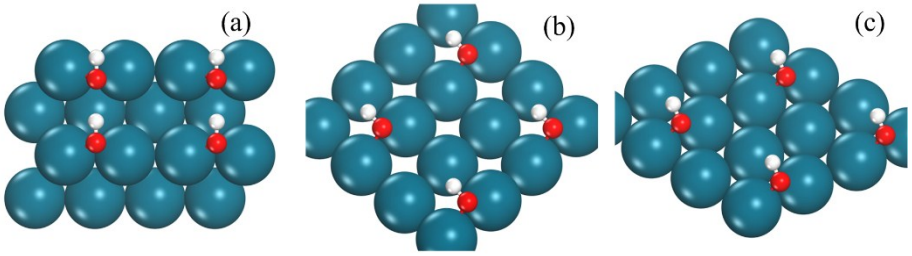

Figure S6. Optimized the most stable structures of the surface adsorbed hydroxyl group on (a) Pd(110), (b) Pd(100) and (c) Pd(111), respectively. Blue: Pd atoms, Red: O atoms, and White: H atoms.

Table S1. The calculated adsorption energies for the OH_{ads} adsorbed (¼ monolayer) on the Pd(110), Pd(100) and Pd(111) surfaces.

Surface	Adsorption Binding Energy (eV)		
	Top	Hollow	**Bridge**
Pd(110)	-2.85	N/A	**-2.90**
Pd(100)	-2.23	-2.55	**-2.70**
Pd(111)	-2.16	-2.28 (hcp) / -2.39 (fcc)	**-2.46**

8. Discussion on the highest electrocatalytic oxidation current density observed for ethanol/ethylene glycol oxidation on Pd Cubes among the three types of Pd catalysts studied

The oxidation mechanisms of ethanol and ethylene glycol on Pd surfaces are very complicated and have so far not been fully established. The oxidation currents showing up are related to many factors including but not limited to the potential and facet dependent adsorption and dehydrogenation of ethanol and ethylene glycol, cleavage of the C-C bonds of adsorbed acteyl (or hydroxylacetly) and adsorption of resulting C1 species, chemisorption of OH, and mobilities of surface species. It is extremely hard if not impossible to give a thorough mechanistic understanding of the observed results in this communication. Nevertheless, the main purpose of this work is firstly to demonstrate shape (nanofacet) dependent electrocatalytic behaviors of EOR and EGOR on Pd nanocrystals, and secondly to give a qualitative explanation of these behaviors, using the two simplified descriptors based on both the literature reports and our own measurements, i.e., the facet dependent dehydrogenation of ethanol and ethylene glycol, together with the facet dependent binding strengths of surface OH and CO chemisorption.

In general, different atomic arrangements and the resulting electronic properties including d-band center may cause facet-sensitive reactivities. Specifically, according to the previous DFT calculation study[16], the dehydrogenation of ethanol occurs most favorably on Pd(100), followed by Pd(110) and Pd (111) in sequence, which to a large extent contributes to the highest oxidation current peak on Pd nanocubes. Also the affinity of chemisorbed OH need to be considered, which is a reactant pair in oxidizing surface C1 and C2 carbonaceous intermediates including CO_{ads}, $CH_3C^*=O$ and $HOCH_2C^*=O$. Our DFT calculation indicates that OH_{ad} forms most favorably on Pd(110), followed by Pd(100) and Pd(111). This may largely explain the lowest onset

oxidation potential observed for EOR and EGOR on Pd RDs. The C-C bond cleavage is mostly favored on Pd(110), forming the CO and CH_x surface species; on the other hand, the mobilities of surface species are expectedly lower on the (110) stepped surface as compared to those on the flat Pd(111) and Pd(100) surfaces, compromising the overall oxidation reaction (i.e., oxidation current density). This may explain the moderate oxidation current density on Pd RDs. Given all the above effects, it is not unreasonable to observe the highest oxidation peak current densities for EOR and EGOR on Pd nanocubes among the three types of Pd nanocatalysts studied in the present work.

9. Discussion on the highest peak potential observed in the voltammograms for the main CO stripping peak on Pd Octs among the three types of Pd catalysts studied

The order of the main CO oxidation peaks on the three different shapes of Pd nanocrystals in the present work is in agreement with that observed by Th. Wandlowski [17] on Pd(111), Pd(110) and Pd(100) single crystal electrodes in acidic media. Moreover, according to *in-situ* IR spectroscopy reported by Takehiko Ogawa[18], hollow site CO or triply bonded CO with the strongest binding can only be detected on Pd(111) rather than on Pd(100) or Pd(110). Both our own and Wandlowski's experimental results have in fact indicated that CO adsorption on Pd(111) (or Pd Octs) is the strongest and thus the CO adsorbate is the hardest to be oxidized among the three basic facets. Further evidence regarding the strongest binding of CO on Pd(111) comes from the comparative DFT calculations on the ease of CO oxidation on Pd(111) and Pd(100) by Hu's group who concluded that a lower barrier for CO oxidation was obtained on Pd(100) than that on Pd(111)[19].

References:

1 H. X. Zhang, H. Wang, Y. S. Re and W. B. Cai, *Chem Commun*, 2012, **48**, 8362-8364.

2 W. X. Niu, L. Zhang and G. B. Xu, *ACS Nano*, 2010, **4**, 1987-1996.

3 J. W. Hong, D. Kim, Y. W. Lee, M. Kim, S. W. Kang and S. W. Han, *Angew Chem Int Edit*, 2011, **50**, 8876-8880.

4 Kresse, J. Hafner, *Phys. Rev. B*, 1993, 48, 13115–13118.

5 G. Kresse, J. Furthmuler, *Phys. Rev. B*, 1996, 54, 11169–11186.

6 G. Kresse, J. Hafner, *Phys. Rev. B,* 1993, 47,558–561.

7 G. Kresse, J. Hafnre, *Phys. Rev. B*,1994, 49, 14251–14269.

8 G. Kresse, J. Furthmuller, *Comput. Mater. Sci.*, 1996, 6, 15–50.

9 P. E. Blochl, *Phys. Rev. B*, 1994, 50, 17953– 17979.

10 G. Kresse, D. Joubert, P*hys. Rev. B*, 1999, 59, 1758–1775.

11 J. P. Pedrew, K. Burke, M. Ernzerhof, *Phys. Rev. Lett.,* 1996, 77, 3865–3868.

12 J. K. Norskov, J. Rossmeisl, A. Logadottir, L. Lindqvist, J. R. Kitchin, T. Bligaard and H. Jonsson, *J.Phys. Chem. B*, 2004, 108, 1520.

13 L. Yu, X. L. Pan, X. M. Cao, P. Hu and X. H. Bao, *J. Catal.*, 2011, 282, 183.

14 F. Colmati, G. Tremiliosi-Filho, E. R. Gonzalez, A. Berna´, E. Herrero and J. M. Feliu, *Faraday Discuss.*, 2008, 140, 379.

15 J. Rossmeisl, J. K. Norskov, C. D. Taylor, M. J. Janik and M. Neurock, *J. Phys. Chem. B*, 2006, 110, 21833.

16 E. D. Wang, J. B. Xu and T. S. Zhao, J Phys Chem C, 2010, 114, 10489-10497.

17 M. Hara, U. Linke and T. Wandlowski, Electrochim Acta, 2007, 52, 5733-5748.

18 N. Hoshi, O. Koga, Y. Hori and T. Ogawa, J Electroanal Chem, 2006, 587, 79-85.

19 C. J. Zhang and P. Hu, J Am Chem Soc, 2001, 123, 1166-1172.